Rotation-vibration model for the chiral doublet bands and wobbling bands in transitional nuclei

H. D. Jiang,[1] Y. Zhang,[1,*] B. Qi,[2] and H. Zhang[2]

[1]*Department of Physics, Liaoning Normal University, Dalian 116029, China*

[2]*Shandong Provincial Key Laboratory of Optical Astronomy and Solar-Terrestrial Environment, School of Space Science and Physics, Institute of Space Sciences, Shandong University, Weihai 264209, China*

(Received 19 March 2024; revised 21 May 2024; accepted 21 August 2024; published 3 September 2024)

A collective model Hamiltonian incorporating a β-soft potential is proposed to elucidate phenomena related to triaxiality in transitional systems. The solutions derived from the model built within the core-particle scheme can be approximated using Bessel functions and subsequently applied to describe the exotic high-spin phenomena observed in the $A \approx 130$ mass region. The results indicate that chiral and wobbling rotations in a β-soft system may exhibit robustness against β vibrations, suggesting a collective vibration mechanism for multiple chiral doublet bands and multiple rotation-wobbling bands in triaxial nuclei.

DOI: 10.1103/PhysRevC.110.034301

I. INTRODUCTION

Spontaneous chiral symmetry breaking in atomic nuclei [1] has attracted intensive investigation since the pioneering work in 1997 [2]. The relevant phenomenon is suggested to occur in a triaxially deformed nucleus with high-j valence particles (holes) configurations. Experimental evidence for this phenomenon, manifested as chiral doublet bands, was initially observed in the $N = 75$ isotopes [3] and subsequently in around 50 nuclei in the $A \approx 80,\ 100,\ 130,\ 190$ regions [4–23]. It was further demonstrated [24] that multiple chiral doublet bands may exist in a single nucleus with different single-particle configuration [25–27] and the experimental evidences have been then reported for nuclei with both odd and even mass number [28–38]. In addition to chiral rotation, wobbling motion [39] is another phenomenon suggested to occur in a triaxially deformed nucleus with high-j valence particles [40–42]. Specifically, wobbling motion describes small amplitude oscillation of the total angular momentum vector with respect to the principal axis with the largest moment of inertia. The experimental signatures were predominantly observed in the odd mass systems in the $A \approx 100,\ 130,\ 160,\ 190$ regions [43–53]. Notably, recent findings [54] have revealed that wobbling motion and chiral rotation may simultaneously occur within a single nucleus, highlighting the complexity of angular momentum coupling in a triaxial system. In short, chirality and wobbling are considered to be two unambiguous fingerprints of triaxiality in nuclei.

On the theoretical side, the particle-rotor model (PRM) [2,8,55–57], the titled axis cranking model [2,58–60], the interacting boson-fermion-fermion model [12,61,62], and the projected shell model [63,64] have been successfully applied to describe chiral rotations in triaxial nuclei. Similar models [40–42,65–69] and methods [70,71] have been also utilized to elucidate wobbling motions. Among them, the PRM offers the most convenient framework for analyzing the two high-spin phenomena linked to triaxiality, and some important concepts were even derived from the theoretical analysis of this model. However, both the β and γ degrees of freedom have been frozen in describing related experiments using the PRM, allowing only the rotational excitations. A more comprehensive consideration of collective motion should commence with the Bohr Hamiltonian [39], especially for the transitional systems associated with β-soft deformations. Although solving the Bohr Hamiltonian usually needs to employ certain approximations [72], new insights into nuclear collective dynamics can often be gleaned from exact or approximate solutions of the model. A prime example is the development of critical point symmetry (CPS) [73,74] for describing nuclear shape phase transitions, where different CPSs are associated with solutions of the Bohr Hamiltonian with different potentials [73–78]. Particularly, a square well potential due to its solvability was frequently employed in the CPS Hamiltonian for modeling a β-soft structure that is expected to be exhibited by transitional nuclei [73]. Additionally, triaxial deformation is anticipated to manifest to some extent in transitional systems such as those in the $A \approx 130$ mass region, where numerous experimental candidates of chiral doublet bands and wobbling bands have been identified [3,9,11,12,28,48,50,51].

In this work, we aim to expand the PRM descriptions of the chiral and wobbling modes by incorporating the Bohr Hamiltonian with a β-soft potential to simulate the transitional cases in triaxial systems containing both even-A and odd-A nucleons. The resulting model can be utilized to examine the impact of β softness on the two exotic nuclear modes associated with triaxiality.

II. THE MODEL

In the core-particle coupling scheme [79], the collective Hamiltonian for an odd-odd system can be expressed as

$$\hat{H} = \hat{H}_c + \hat{H}_p + \hat{H}_n\,, \tag{1}$$

*Contact author: dlzhangyu_physics@163.com

where $\hat{H}_c$ represents the Bohr Hamiltonian for the even-even core and $\hat{H}_\sigma$ with $\sigma = p, n$ represents the single-particle Hamiltonian for the odd nucleon (unpaired proton or neutron). It is assumed that there is no additional interaction between the core and odd nucleons except for the correlation in the angular momentum coupling with $\hat{I} = \hat{L} + \hat{j}_p + \hat{j}_n$, where $\hat{L}$, $\hat{j}_p$, $\hat{j}_n$, and $\hat{I}$ represent the angular momentum operators for the even-even core, odd proton, odd neutron and whole odd-odd system. This assumption is commonly employed in the PRM calculations and has been demonstrated to work well when dealing with odd nucleons occupying high-j orbits [79]. In fact, if the β and γ degrees of freedom are frozen, then the collective Hamiltonian in Eq. (1) will be reduced to that of the PRM [55].

For a transitional odd-odd system, the core dynamic can be approximately described by the T(4) CPS [80], which is motivated by the model of Davydov and Chaban with a fixed γ degree of freedom [81]. Specifically, the Bohr Hamiltonian for the even-even core is written by

$$\hat{H}_c = -\frac{\hbar^2}{2B}\left[\frac{1}{\beta^3}\frac{\partial}{\partial\beta}\beta^3\frac{\partial}{\partial\beta} - \frac{1}{4\beta^2}\sum_k \frac{\hat{L}_k^2}{\sin^2\left(\gamma - \frac{2}{3}k\pi\right)}\right] + V(\beta), \tag{2}$$

where β is the collective variable, B is the collective mass parameter, and $\hat{L}_k$ $(k = 1, 2, 3)$ represents the projection of the core angular momentum on the body-fixed k axis. To simulate a β-soft structure, the potential function is designed to be the infinite square well in β,

$$V(\beta) = \begin{cases} 0, & \beta \leqslant \beta_W, \\ \infty, & \beta > \beta_W. \end{cases} \tag{3}$$

Such a Hamiltonian can be solved like the rotor model [80], given that γ is treated here as a parameter characterizing axial asymmetry.

For the single-particle part, we restrict the odd nucleon (unpaired proton or neutron) to a single-j shell. The single-particle Hamiltonian in the intrinsic frame of the core deformation can be expressed as [79]

$$\hat{H}_\sigma = \hat{H}_0 + kr^2\beta\left[\cos(\gamma)Y_{20} + \frac{\sin(\gamma)}{\sqrt{2}}(Y_{22} + Y_{2-2})\right], \tag{4}$$

where the spherical shell term $\hat{H}_0$ corresponds to the spherical harmonic oscillator and the second term describes the quadrupole deformation of the single-particle potential with the parameter k given by the splitting of the j shell in the Nilsson scheme under the deformations of β and γ. For high j shells, the single-particle Hamiltonian in Eq. (4) is rewritten as [79]

$$\hat{H}_p + \hat{H}_n = E_0 + \sum_{\sigma=p,n} C_\sigma\left\{\left[\hat{j}_{\sigma 3}^2 - \frac{j_\sigma(j_\sigma+1)}{3}\right]\cos(\gamma) + \frac{1}{2\sqrt{3}}\left[\hat{j}_{\sigma+}^2 + \hat{j}_{\sigma-}^2\right]\sin(\gamma)\right\}, \tag{5}$$

with $\hat{j}_{\sigma\pm} = \hat{j}_{\sigma 1} \pm i\hat{j}_{\sigma 2}$. The first term E_0 arises from a constant contribution of the spherical shell term $\langle\hat{H}_0\rangle$ for the given single-j orbits, while the second and third terms describe level splitting due to the axial asymmetry of the potential field. In the concrete calculations, the strength parameter C_σ (in MeV) is often taken by the form

$$C_\sigma = \pm\frac{195}{2j_\sigma(j_\sigma+1)}A^{-1/3}\beta, \tag{6}$$

in which the plus sign refers to a particle and the minus to a hole. The single-particle Hamiltonian form presented in Eq. (5) aligns with the one frequently adopted in the PRM [55,56].

To solve the model Hamiltonian, one can make an approximate separation of the variables by introducing the reduced energy $\epsilon = 2BE/\hbar^2$, the reduced potential $u = 2BV/\hbar^2$ and the reduced single-particle energy $\hat{h}_{\rm sp} = 2B\beta^2\hat{H}_{\rm sp}/\hbar^2$ with the involved β^3 being approximately replaced by $\overline{\beta^3} = \langle\beta^3\rangle_g$. Here $\overline{\beta^3}$ represents the average value of β^3 over $\eta(\beta)$ solved from Eq. (8), which is defined below, for the lowest state. This is equivalent to an assumption that the strength parameter in Eq. (6) satisfies $C_\sigma \sim a/\beta^2$ and the adjustable parameter "a" is then approximately determined by $a \simeq \langle\beta^3\rangle_g$ in order to be in accord with the widely used form in the PRM calculations [55]. The similar approximation has been previously employed in solving the CPS models associated with the infinite square well potential [74–77]. Subsequently, the eigenvalue equation $\hat{H}\Psi = E\Psi$ can be separated into two equations, i.e., the rotational equation

$$\left[\sum_{k=1}^{3}\frac{\hat{L}_k^2}{4\sin^2\left(\gamma - \frac{2}{3}k\pi\right)} + \hat{h}_{\rm sp}\right]\varphi(\theta_i, a_p, a_n) = r\varphi(\theta_i, a_p, a_n) \tag{7}$$

with r denoting its eigenvalues and the vibrational equation

$$\left[-\frac{1}{\beta^3}\frac{\partial}{\partial\beta}\beta^3\frac{\partial}{\partial\beta} + \frac{r}{\beta^2} + u(\beta)\right]\eta(\beta) = \varepsilon\eta(\beta) \tag{8}$$

with ε denoting its eigenvalues. The total wave function is then expressed as

$$\Psi = \eta(\beta)\varphi(\theta_i, a_p, a_n), \tag{9}$$

where θ_i $(i = 1, 2, 3)$ are the Euler angles and $a_{p(n)}$ represents generally the coordinates of the odd proton (neutron).

The single particle Hamiltonian may directly influence the collective rotation of the system as indicated by Eq. (7), which is actually consistent with the one constructed from the PRM [79]. To solve the rotational equation, one can expand the rotational wave function as

$$\varphi^I_{M,s}(\theta_i, a_p, a_n) = \sum_{K,\Omega_p,\Omega_n} C^{I,K}_{s,\Omega_p,\Omega_n}\chi^{I,K}_{M,\Omega_p,\Omega_n}(\theta_i, a_p, a_n) \tag{10}$$

with

$$\chi^{I,K}_{M,\Omega_p,\Omega_n} = \sqrt{\frac{2I+1}{16\pi^2}}\left[D^I_{M,K}(\theta_i)\phi^{j_p}_{\Omega_p}(a_p)\phi^{j_n}_{\Omega_n}(a_n) + (-1)^{I-j_p-j_n}D^I_{M,-K}(\theta_i)\phi^{j_p}_{-\Omega_p}(a_p)\phi^{j_n}_{-\Omega_n}(a_n)\right], \tag{11}$$

where $D^I_{M,K}(\theta_i)$ is the Wigner D-function and $\phi^j_\Omega(a)$ is the single-particle wave function with Ω denoting the component of the spin j on the intrinsic z axis, while s is an additional

quantum number used to distinguish between states with the same I, M. The symmetry in question is the D2h symmetry. Due to the symmetry constraint [55], the summation in Eq. (10) is restricted to $K = 0,\ 1,\ 2, \ldots, I$ with $K - \Omega_p - \Omega_n$ being even numbers and $\Omega_p > 0$ when $K = 0$. The expansion coefficients $C^{I,K}_{s,\Omega_p,\Omega_n}$ are then determined by Eq. (7) along with the corresponding eigenvalues denoted by r^I_s. Since the constant term E_0 in Eq. (5) will not change the eigenvalue structure of Eq. (7), its value will be simply fixed such that the lowest eigenvalue holds $r_{\min} = 0$ to ensure that rotational excitation energies are larger than zero. This point agrees with the rotor model calculations for even-even system. With the r^I_s value determined from Eq. (7), one can transform the β-vibrational equation inside the infinite well as given in Eq. (8) into the Bessel equation

$$\frac{d^2F}{dz^2} + \frac{1}{z}\frac{dF}{dz} + \left[1 - \frac{v^2}{z^2}\right]F = 0 \tag{12}$$

with the order $v = (r^I_s + 1)^{1/2}$, where we have taken $F(\beta) = \beta\eta(\beta)$ and $z = \beta k$ with $k = \sqrt{\epsilon}$. The boundary condition $\eta(\beta_W) = 0$ is used to determine eigenvalues and eigenfunctions, which are expressed as

$$\epsilon_{\xi,s,I} = (k_{\xi,v})^2, \quad k_{\xi,v} = \left(\frac{x_{\xi,v}}{\beta_W}\right), \tag{13}$$

and

$$\eta_{\xi,s,I}(\beta) = c_{\xi,v}\beta^{-1}J_v(k_{\xi,v}\beta) \tag{14}$$

with $x_{\xi,v}$ denoting the ξth zero of the Bessel function $J_v(z)$. Accordingly, the normalization constants $c_{\xi,v}$ are determined by

$$\int_0^{\beta_W} \beta^3\eta^2_{\xi,s,I}(\beta)d\beta = 1\,. \tag{15}$$

The total energy is finally expressed as

$$E(\xi, s, I) = \frac{\hbar^2}{2B}(k_{\xi,v})^2\,. \tag{16}$$

Clearly, the order of Bessel functions v plays a pivotal role as its values completely determine the model structure. It is evident that different excitation states in the model can be characterized by different values of I, ξ, and s. For instance, the lowest rotational band is associated with $\xi = 1$ and $s = 1$, while the bands related to β vibrations is characterized by $\xi = 2,\ 3, \ldots$.

To calculate the $B(E2)$ transitional rates, the $E2$ operator is chosen by

$$\hat{T}^{E2}_u = \sqrt{\frac{5}{16\pi}}Q_0\Big[\cos(\gamma)D^{(2)}_{u,0}(\theta_i) + \frac{\sin(\gamma)}{\sqrt{2}}\left(D^{(2)}_{u,2}(\theta_i) + D^{(2)}_{u,-2}(\theta_i)\right)\Big], \tag{17}$$

where Q_0 denotes the intrinsic quadrupole moment. In the concrete calculations, we adopt the empirical formula

$$Q_0 = \frac{3}{\sqrt{5\pi}}R_0^2Z\beta, \quad R_0 = 1.3A^{1/3}\,, \tag{18}$$

in which Z denotes the charge number and R_0 represents the average nuclear radius (unit in fm). The reduced $B(E2)$ transitional rates can then be calculated via

$$B(E2; \alpha_i, I_i \to \alpha_f, I_f) = \frac{|\langle\alpha_f, I_f \parallel \hat{T}^{E2} \parallel \alpha_i, I_i\rangle|^2}{2I_i + 1}\,, \tag{19}$$

where α represents generally all the quantum numbers in addition to I. In the calculations, the integral over β takes the form

$$K_\beta(\xi_i, s_i, I_i;\ \xi_f, s_f, I_f) = \int_0^{\beta_w} \beta\eta_{\xi_i,s_i,I_i}(\beta)\eta_{\xi_f,s_f,I_f}(\beta)\beta^3 d\beta\,, \tag{20}$$

and the integral over the Euler angles θ_i is achieved by employing the formula that involves three Wigner D-functions. The final results can be expressed as

$$\begin{aligned} B\big(E2; I_{i\xi_i,s_i} \to I_{f\xi_f,s_f}\big) &= \frac{9}{16\pi^2}(R_0^2Z)^2K^2_\beta(\xi_i, s_i, I_i;\ \xi_f, s_f, I_f) \\ &\times\Bigg\{\sum_{K_i,K_f,\Omega_p,\Omega_n} C^{I_i,K_i}_{s_i,\Omega_p,\Omega_n}C^{I_f,K_f}_{s_f,\Omega_p,\Omega_n} \\ &\times\Bigg[\cos(\gamma)\langle 20I_iK_i|I_fK_f\rangle + \frac{1}{\sqrt{2}}\sin(\gamma)\langle 2 - 2I_iK_i|I_fK_f\rangle \\ &+\frac{1}{\sqrt{2}}\sin(\gamma)\langle 22I_iK_i|I_fK_f\rangle\Bigg] + \cdots\Bigg\}^2\,, \end{aligned} \tag{21}$$

where "…" represents the other terms [56]. Similarly, the $M1$ transition can be calculated using the magnetic dipole operator defined by [56]

$$\hat{T}^{M1}_u = \sqrt{\frac{3}{4\pi}}\frac{e\hbar}{2Mc}[(g_p - g_R)\hat{j}_{pu} + (g_n - g_R)\hat{j}_{nu}]\,, \tag{22}$$

where g_p, g_n, and g_R denote the effective g factors for proton, neutron and even-even core, while $\hat{j}_u$ denotes the spherical tensor in the laboratory frame. The reduced $B(M1)$ transitional rates are then evaluated via

$$B(M1; \alpha_i, I_i \to \alpha_f, I_f) = \frac{|\ \langle\alpha_f, I_f \parallel \hat{T}^{M1} \parallel \alpha_i, I_i\rangle\ |^2}{2I_i + 1}\,. \tag{23}$$

Throughout this work, the g factors are set to $g_p - g_R = 0.7$ and $g_n - g_R = -0.6$ [56]. If applying the $M1$ operator defined in Eq. (22) to odd-A systems, then only the first or second term is needed, depending the valence nucleon being a single proton or neutron [82].

The core-particle coupling Hamiltonian in Eq. (1) for odd-A system contains either H_p or H_n, with the total angular momentum given by $\hat{I} = \hat{L} + \hat{j}_{p(\text{or}\,n)}$. The steps for solving the odd-A Hamiltonian would be very similar to the ones for the odd-odd case described above, which means that the eigenfunctions and eigenvalues may have the same forms as those shown in Eq. (9) and Eq. (16). In subsequent discussion, we omit the derivations for odd-A cases and just describe the calculated results. Since only the three parameters, B, β_W, and

γ, are adjustable for the neighboring even-even, odd-A and odd-odd systems, the present model may provide a chance to examine the core-particle coupling scheme in the corresponding way.

III. RESULTS AND DISCUSSIONS

As discussed in Ref. [83], the core Hamiltonian taken from the T(4) CPS [80] may exhibit characteristics of a β-soft rotor. Its solutions as a function of the deformation parameter γ can offer a comprehensive description of the transitional even-even nuclei, ranging from the first-order shape phase transition as observed in rare-earth nuclei with $A \approx 150$ to the second-order shape phase transition seen in the $A = 130$ mass region. Interestingly, the phenomena related to chiral rotation and wobbling motion have also been observed in the $A = 130$ region [3,22,50,51]. To demonstrate the model application, we choose the Xe, Ba isotopes and their adjacent partners in this mass region to conduct the relevant theoretical calculations.

A. Even-even nuclei

For the even-even core described by Eq. (2), the entire level structure (up to a scale factor) will be completely determined by the γ parameter, which is highly sensitive to the ratio of $E(2_\gamma)/E(2_1)$. Here, $E(2_\gamma)$ denotes the band head energy of the γ band. This implies that the energy ratio in the present model can play a role similar to γ in characterizing axial asymmetry. Consequently, one can identify nuclei that better conform to the model dynamics by comparing quantities such as $E(4_1)/E(2_1)$ and $E(8_1)/E(0_2)$ as they evolve with $E(2_\gamma)/E(2_1)$, both experimentally and theoretically. The specific results are presented in Fig. 1. As seen from Fig. 1(a), the theoretical values of $E(4_1)/E(2_1)$ may monotonically increase with those of $E(2_\gamma)/E(2_1)$, which is similar to the evolutional behaviors observed in the Xe, Ba isotopes. By comparison, the data for ^{126}Xe and ^{132}Ba are closer to the theoretical trajectory. In addition, the results shown in the inset indicate that the rotor model may yield a more rigid spectrum with $E(4_1)/E(2_1) > 2.66$, suggesting that a β-soft core described by the present model may be more suitable for these transitional nuclei. As further observed from Fig. 1(b), the theoretical values of $E(8_1)/E(0_2)$ as a function of $E(2_\gamma)/E(2_1)$ is nearly constant, effectively reproducing the results for ^{126}Xe and ^{132}Ba. It is thus confirmed that the properties of the nuclei can indeed be described by the model. Based on the results shown in Fig. 1, one can also estimate the γ values to be used in the model calculations, which are suggested to be $\gamma = 22^\circ$ and $\gamma = 23^\circ$ for ^{126}Xe and ^{132}Ba, respectively.

To determine the remaining two parameters, B and β_W, the low-lying levels and available $B(E2)$ data in the two nuclei are fitted by the model calculations. As seen from Fig. 2, the level patterns of both nuclei can be well reproduced in theory especially for the γ- and β-band head energies as indicated by the corresponding ratios. A discrepancy aries from the relatively small energy gaps between 3_1^+ and 4_2^+ in experiments, suggesting that γ deformation of the two nuclei may be more or less softer. In addition, the state 2_4^+ rather than 2_3^+ in ^{132}Ba can be arranged as the band member of the 0_2^+

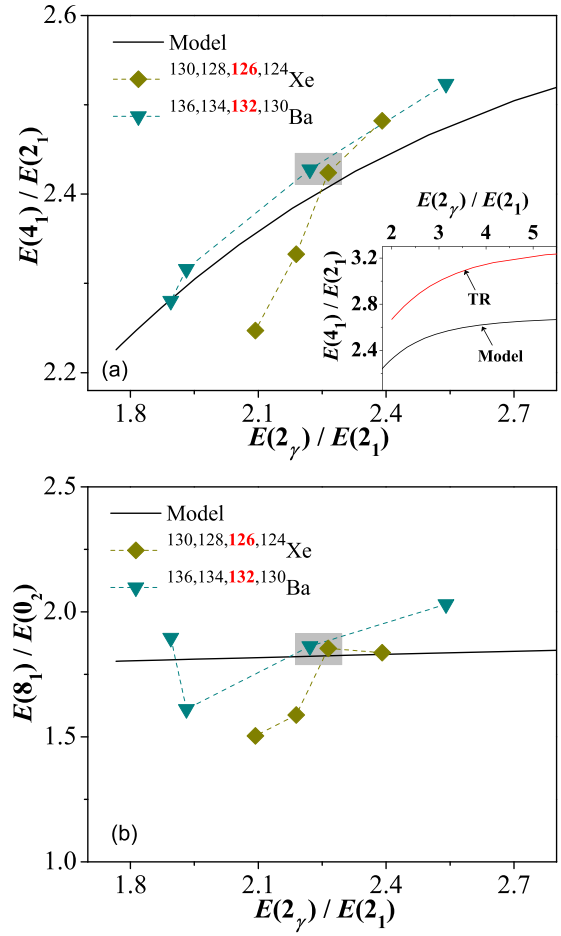

FIG. 1. The energy ratios $E(4_1)/E(2_1)$ and $E(8_1)/E(0_2)$ obtained from the model are presented as a function of $E(2_\gamma)/E(2_1)$ for comparison with the experimental data extracted from the Ba and Xe isotopes [84–89]. The inset provides a comparison between the results for $E(4_1)/E(2_1)$ vs $E(2_\gamma)/E(2_1)$ derived from the present model and those from the triaxial rotor model (TR) using the hydrodynamical moments of inertia.

band according to the analysis given in Ref. [90]. As shown in Table I, the available data for $B(E2)$ transitions can also be generally well described by theory, except for the overestimation of $B(E2; 0_2 \to 2_1)$ in ^{126}Xe. This discrepancy could also be improved through incorporating a softer potential in γ.

B. Odd-odd nuclei

Based on the above analysis, the two even-even nuclei that best conform to the model predictions both exhibit the large triaxial deformations with $\gamma > 20^\circ$. For odd-odd nuclei, chiral doublet bands originating from spontaneous chiral symmetry breaking serve as a crucial indicator of triaxial deformation. In experiments, chiral bands were mostly observed in the triaxial odd-odd nuclei with the valence particles (holes) occupying high-j orbits. To illustrate this triaxiality-related phenomenon, the single-particle configuration is chosen to be $\pi h_{11/2} \otimes \nu h_{11/2}^{-1}$ with the strength parameters $C_{\pi(\nu)}$ determined from Eq. (6). Then, the high-spin structures derived

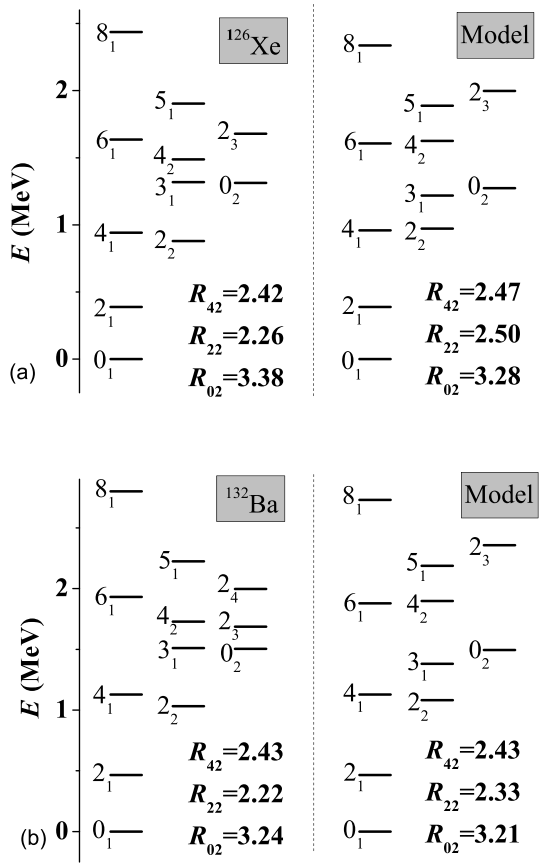

FIG. 2. The patterns of low-lying excitation states for ^{132}Ba and ^{126}Xe are provided to compare with the results solved from the core Hamiltonian with the model parameters given in Table I. The typical energy ratios are defined as $R_{42} = E(4_1)/E(2_1)$, $R_{22} = E(2_2)/E(2_1)$, and $R_{02} = E(0_2)/E(2_1)$.

from this single-particle configuration in an odd-odd nucleus will be completely fixed in theory, as all the model parameters have been determined by reproducing the low-lying properties of the adjacent even-even nucleus. The odd-odd partners of ^{126}Xe and ^{132}Ba satisfying one particle one hole condition are identified as ^{126}Cs [22] and ^{132}La [91], respectively. They will be taken in the following to examine the model predictions under the given parameters. For that, the level patterns solved from Eq. (1) are shown in Fig. 3 to compare with the experimental results for the yrast bands and yrare bands built on $\pi h_{11/2} \otimes \nu h^{-1}_{11/2}$. Besides, the calculated energy staggering parameter $S(I)$ and $B(M1)/B(E2)$ ratios are shown in Fig. 4 and Fig. 5, facilitating further comparison in between theory and experiment.

As seen in Fig. 3(a), the level energies of the yrast and yrare bands in ^{126}Cs can be reasonably reproduced by the model results characterized by $\xi = 1$ and $s = 1, 2$. In particular, the near degeneracies in the levels of the same spins can be clearly observed in both the experimental data and the theoretical results for the two $\Delta I = 1$ bands, especially for $I > 12$. It is thus suggested that the yrast band and yrare band form a pair of chiral doublet bands [22]. An agreement between the experiment and theory can also be found for ^{132}La as depicted in Fig. 3(b). Similarly, the yrast and yrare bands in this nucleus also constitute a pair of chiral doublet bands with near degeneracies present in the levels of the same spins. A chiral interpretation of the two bands in ^{132}La has also been provided in the previous study [6]. Additionally, the results in Fig. 3 indicate that the present model may yield a patten featuring multiple doublet bands arising from collective excitations, including the bands denoted by $\xi = 2$ alongside $s = 1, 2$, as well as those denoted by $\xi = 1$ together with $s = 3, 4$. By comparing the band head energies between the odd-odd and even-even nuclei, one can derive that the former ($\xi = 2$) corresponds to the β band and the latter ($\xi = 1$) to the γ band. Further analysis of these doublets resulting from collective excitations will be presented below.

TABLE I. The available data for $B(E2)$ transitions (in W.u.) in ^{126}Xe [88] and ^{132}Ba [85] are provided to compare with the results obtained from the model, where "—" denotes unknown data. In the calculations for ^{126}Xe (^{132}Ba), a value of $\gamma = 22^\circ$ (23°) is adopted, the mass parameter (in MeV$^{-1}\hbar$) is taken as $B = 184.6$ (198.9), and the well width is set by $\beta_W = 0.271$ (0.241). With these parameters, the first excited level in the model has been set to precisely match the experimental data for ^{126}Xe (^{132}Ba), which implies $E(2_1) =$ 0.389(0.465) MeV.

$L_i \to L_f$	^{126}Xe	Model	$L_i \to L_f$	^{132}Ba	Model
$2_1 \to 0_1$	44(4)	36	$2_1 \to 0_1$	43(4)	31
$4_1 \to 2_1$	76(12)	65	$4_1 \to 2_1$	–	55
$6_1 \to 4_1$	89(16)	90	$6_1 \to 4_1$	–	77
$0_2 \to 2_1$	6.4(12)	39	$0_2 \to 2_1$	–	34
$2_2 \to 2_1$	47(9)	24	$2_2 \to 2_1$	144(14)	25
$2_2 \to 0_1$	0.68(12)	2.45	$2_2 \to 0_1$	3.9(4)	1.93
$2_3 \to 0_2$	40(6)	28	$2_3 \to 0_2$	–	24

Apart from the near degeneracies in level energies, the other fingerprints of nuclear chirality include the constant evolution of $S(I) = [E(I) - E(I-1)]/2I$ and the staggering in $B(M1)/B(E2) = B(M1; I \to I-1)/B(E2; I \to I-2)$ as these quantities vary with spins. As shown in Fig. 4(a), a nearly constant behavior of $S(I)$ is observed from the data for ^{126}Cs, particularly for $I > 12$, which is also well captured by the model results, thereby reaffirming the chiral rotational nature of the doublet bands in this nucleus. The similar feature can also be discerned for ^{132}La as seen in Fig. 4(b). On the other hand, the calculated results of $S(I)$ exhibit a staggering behavior for large values of I. The staggering feature was also found in the results obtained from the PRM [92], indicating a potential influence from the Coriolis effect at high spins. But, we observe that the staggering feature in the present model appears to be weaker than that in the PRM calculations, suggesting a possible reduction of the Coriolis effect due to β softness. As further seen from Fig. 5, the data for $B(M1)/B(E2)$ in ^{126}Cs can also be reasonably explained by the model calculations. Notably, these ratios in the experiment demonstrate pronounced staggering along the yrast band but weaker staggering along the yrare band. These features are consistent well with the model prediction. For ^{132}La, although the predicted staggering amplitudes for the yrast band appear evidently larger than the experimental observations at

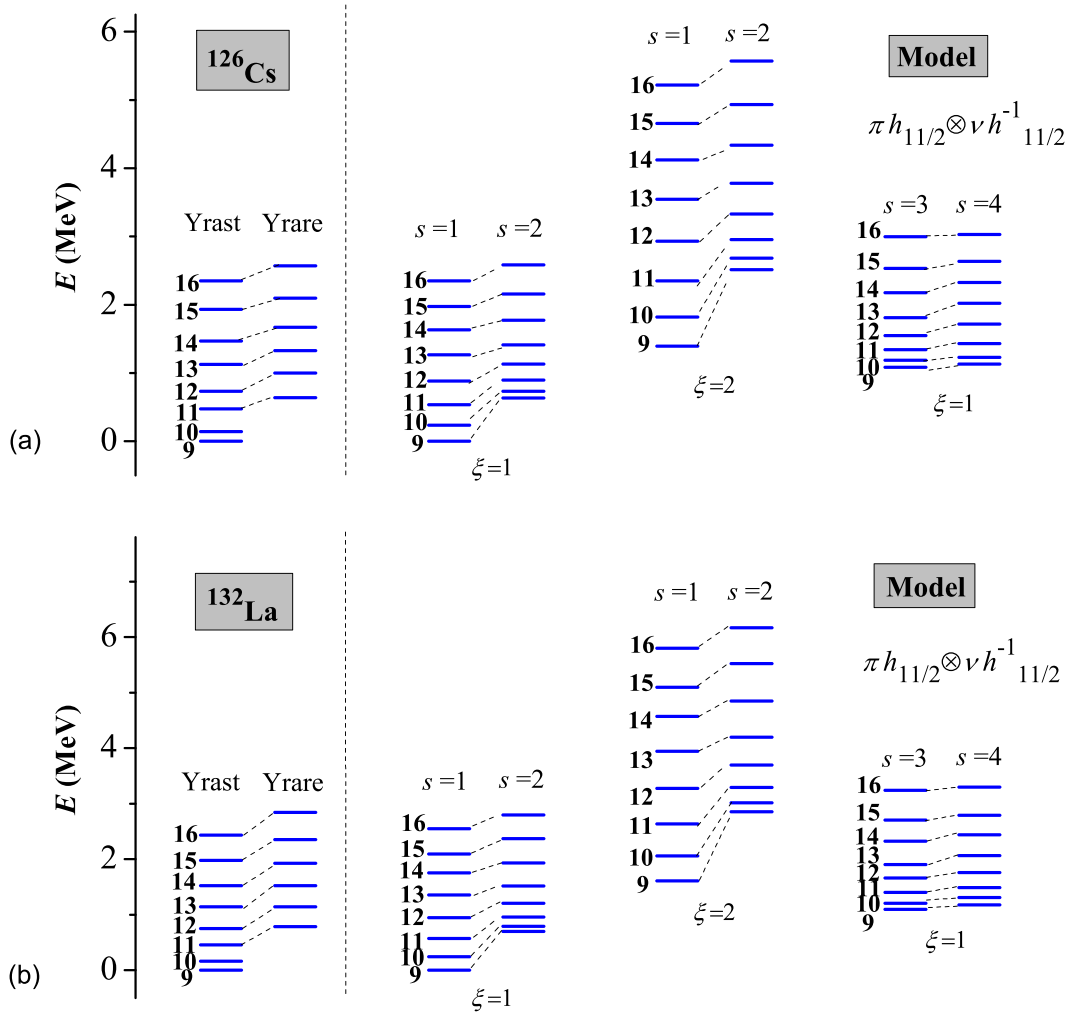

FIG. 3. The patterns of low-lying excitation states for ^{126}Cs [22] and ^{132}La [91] are presented to compare with the results obtained from the model, where $\xi = 1$ and $\xi = 2$ correspond to the lowest bands and β-vibrational bands, respectively, and $s = 1,\ 2,\ 3,\ 4,\ \cdots$ is the additional quantum number to distinguish between states with the same $I,\ M$.

high spins, qualitative agreement in the evolutional trends of $B(M1)/B(E2)$ can still be discerned as shown in Fig. 5(b). Since only one data is available for the yrare band as seen in Fig. 5(d), further measurements of $B(M1)/B(E2)$ in ^{132}La are necessary to enable a reliable comparison between the experiment and theory. The above analysis clearly demonstrates that the two lowest $\Delta I = 1$ bands in both odd-odd nuclei can be attributed to chiral doublet bands, and their characteristics can be identified through the theoretical calculations using the parameters determined from fitting the adjacent even-even nuclei.

To further investigate the properties of the additional doublet bands generated in the model, we select the bands depicted in Fig. 3(a) to examine the evolutional behaviors of $S(I)$ and $B(M1)/B(E2)$ as shown in Fig. 6. As seen from Fig. 6(a), the global features of $S(I)$ for the bands with $\xi = 2$ and $s = 1,\ 2$ are very similar to those exhibited by the yrast and yrare bands shown in Fig. 4(a). The similarities between these two pairs of doublets can also be identified from the evolutions of the $B(M1)/B(E2)$ ratios as observed in Fig. 6(c). It is shown that both the staggering amplitudes and evolutional trends in the doublets with $\xi = 2$ closely mirror those seen in the yrast and yrare bands, which means that the two bands with $\xi = 2$ indeed form a pair of chiral doublet bands. One can thus conclude that chiral rotation within a β-soft system remains robust against β vibrations. In comparison, as depicted in Fig. 6(b) and 6(d), the evolutions of $S(I)$ and $B(M1)/B(E2)$ for the bands with $\xi = 1$ and $s = 3,\ 4$ exhibit fewer similarities to those observed for the yrast and yrare bands.

Examination of the geometry of angular momentum coupling, which can be achieved by analyzing the effective angles between different angular momentum vectors, is essential for a deeper understanding of chiral bands. To this end, we calculate the expectation values of some scalar operators as considered in Ref. [6], including $\langle\,|\hat{L}^2|\,\rangle$, $\langle\,|\hat{L}\cdot\hat{j}_p|\,\rangle$, $\langle\,|\hat{L}\cdot\hat{j}_n|\,\rangle$, and $\langle\,|\hat{j}_p\cdot\hat{j}_n|\,\rangle$, in which $|\,\rangle \equiv |I,\xi,s\rangle$ denote the eigenvectors described by Eq. (9). By utilizing the tensor properties of the angular momentum operators with $\hat{L}_\pm = \hat{L}_1 \pm i\hat{L}_2$, $\hat{j}_\pm = \hat{j}_1 \pm i\hat{j}_2$, and $\hat{I} = \hat{L} + \hat{j}_p + \hat{j}_n$ [79], one can evaluate the expectation values of these scalar operators in a given wave

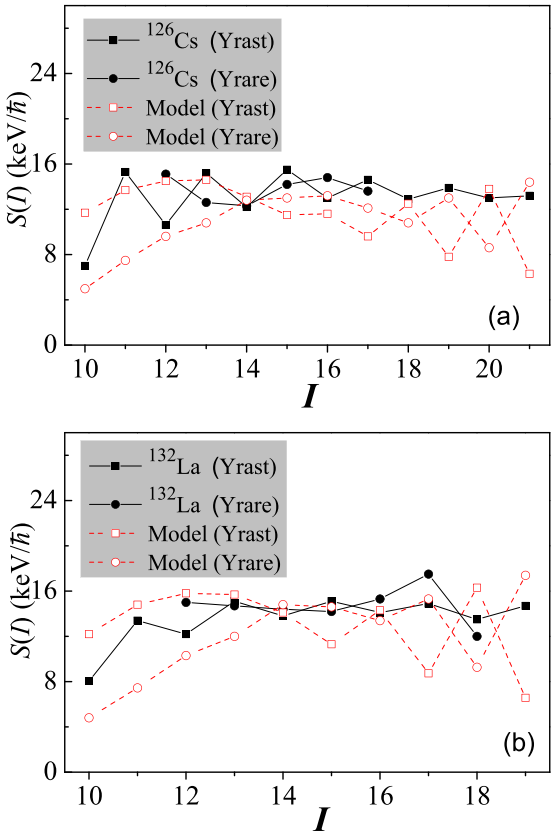

FIG. 4. The energy staggering parameter $S(I)$ for ^{126}Cs [22] and ^{132}La [91] are provided to compare with the results derived from the model, where "yrast" and "yrare" denote those calculated for $\xi = 1$ but with $s = 1$ and $s = 2$, respectively.

function, of which the rotational part can be expanded in terms of the strong-coupling basis as indicated in Eq. (10). These scalars further allow us to define the effective angles with their cosine functions written by [6]

$$\cos(\theta_{Lj_p}) = \frac{\langle \hat{L} \cdot \hat{j}_p \rangle}{\sqrt{\langle \hat{L}^2 \rangle \langle \hat{j}_p^2 \rangle}}, \tag{24}$$

$$\cos(\theta_{Lj_n}) = \frac{\langle \hat{L} \cdot \hat{j}_n \rangle}{\sqrt{\langle \hat{L}^2 \rangle \langle \hat{j}_n^2 \rangle}}, \tag{25}$$

$$\cos(\theta_{j_p j_n}) = \frac{\langle \hat{j}_p \cdot \hat{j}_n \rangle}{\sqrt{\langle \hat{j}_p^2 \rangle \langle \hat{j}_n^2 \rangle}}. \tag{26}$$

Note that the calculated results are independent of the β vibration and, consequently, the values of ξ. This is due to the fact that the β part of the wave functions in the model only contributes an orthonormality factor. It means that the doublet bands denoted by ($\xi = 1$, $s = 1, 2$) and those by ($\xi = 2$, $s = 1, 2$) as depicted in Fig. 3(a) will exhibit identical effective angles in angular momentum coupling. Given that the results depend solely on the quantum number s and I, the angles for

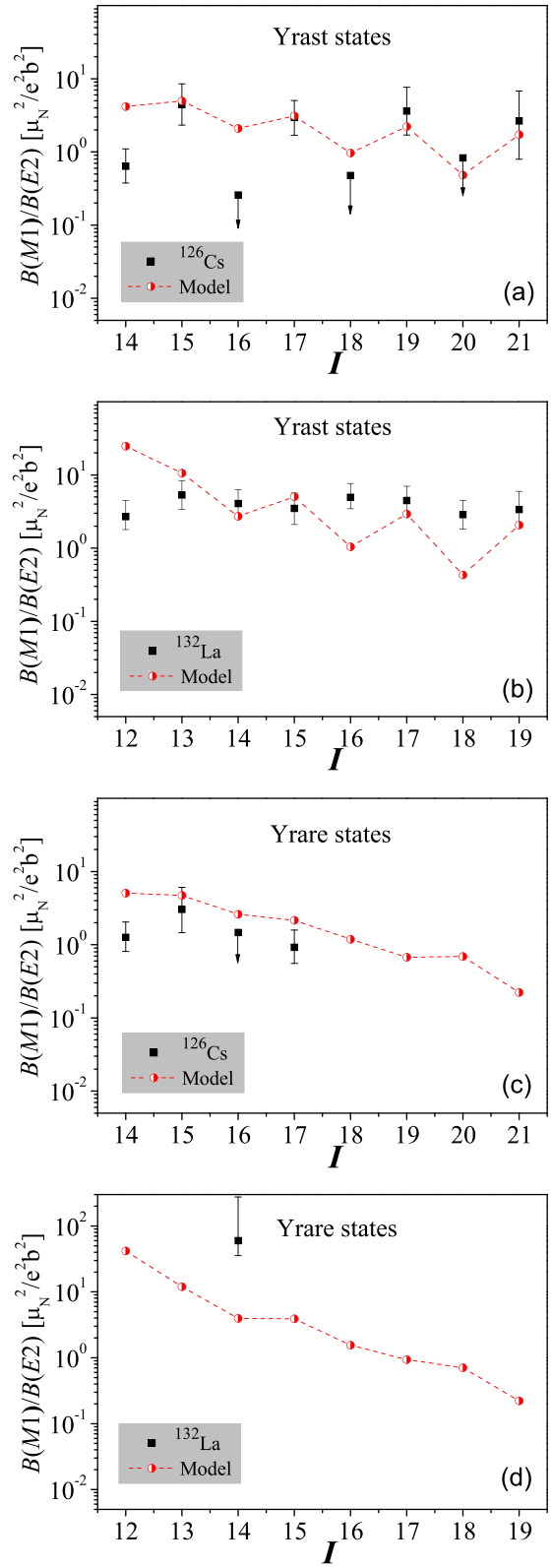

FIG. 5. The evolutions of the $B(M1)/B(E2)$ ratios for the yrast band and yrare band in ^{126}Cs [22] and ^{132}La [91] are shown to compare with those derived from the model.

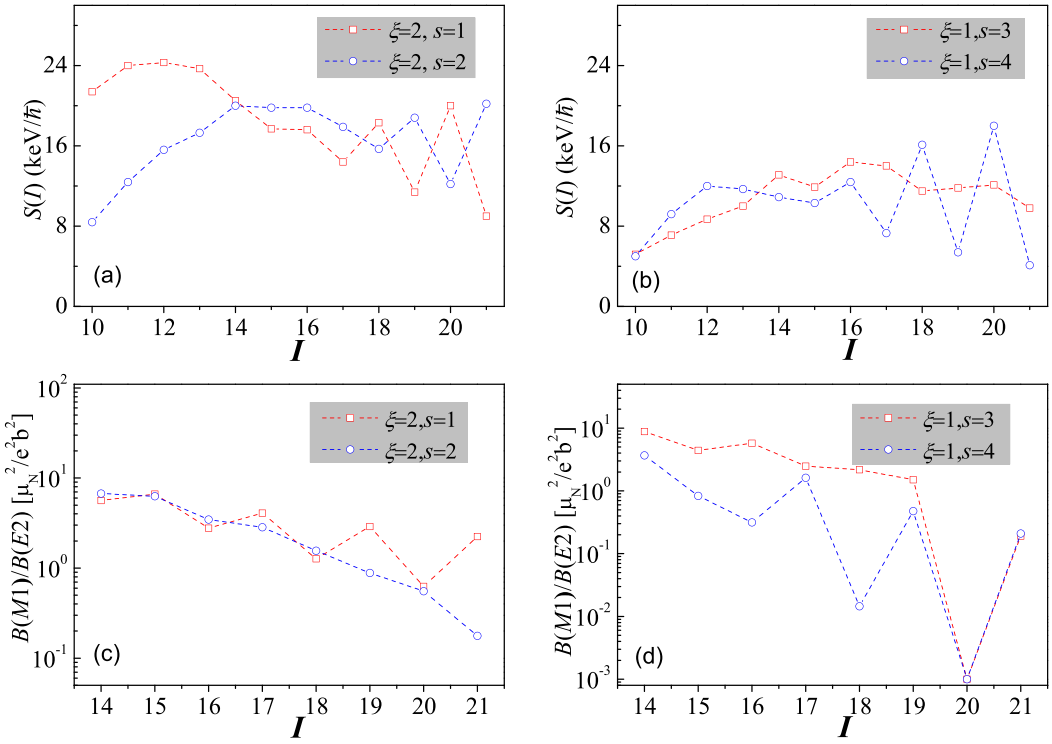

FIG. 6. The theoretical values of $S(I)$ and $B(M1)/B(E2)$ are presented as a function of spin. Here, $\xi = 1, 2$ and $s = 1,\ 2,\ 3,\ 4$ denote the results corresponding to the bands depicted in Fig. 3(a).

$s = 1,\ 2$ are presented as a function of I to compare with those for $s = 3,\ 4$. As illustrated in Fig. 7, the three effective angles for both $s = 1$ and $s = 2$ may decrease from $\theta \approx 90^\circ$ to lower values with increasing spin. Nevertheless, these angle values during their evolutional process remain relatively large, even with some oscillation at high spins. For instance, all three angles exceed 60° for $I \leqslant 14$, except for the angle between $\hat{L}$ and $\hat{j}_p$ for $s = 1$, which yields $\theta_{Lj_p} \approx 48^\circ$ at $I = 14$, as observed in

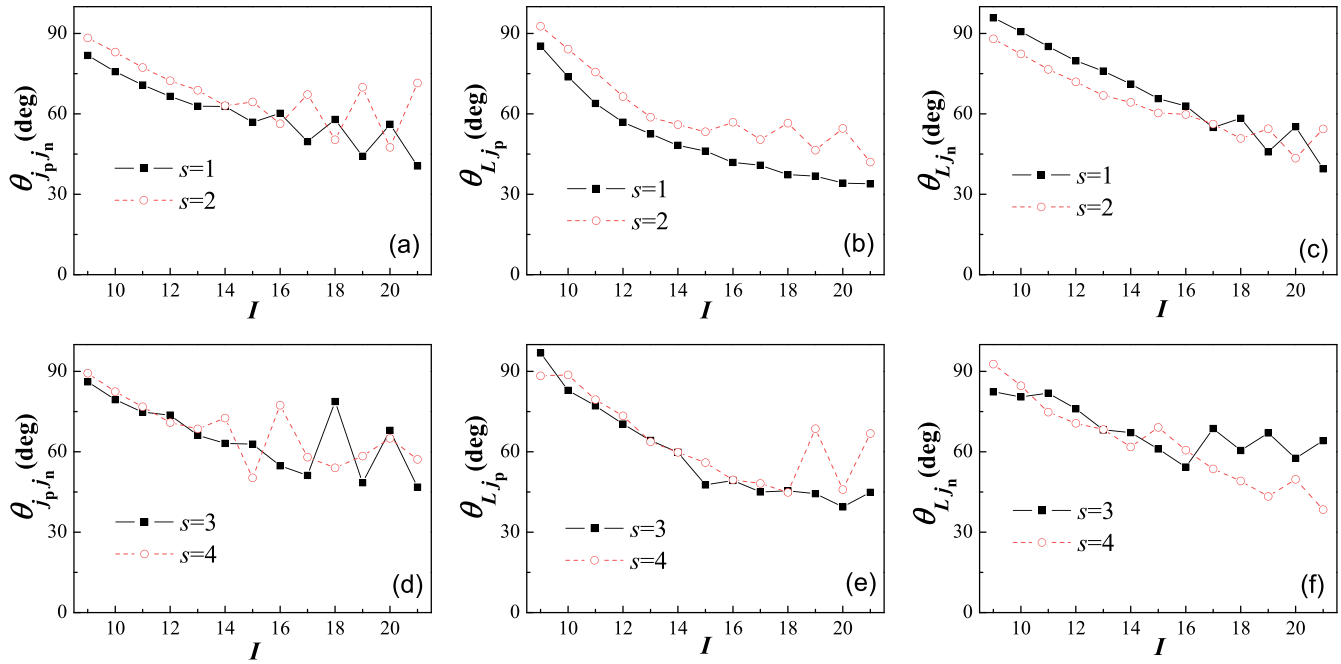

FIG. 7. The effective angles (in degree) between different angular momentum vectors are presented as a function of spin with $(s = 1,\ 2)$ and $(s = 3,\ 4)$ denoting the corresponding bands depicted in Fig. 3(a).

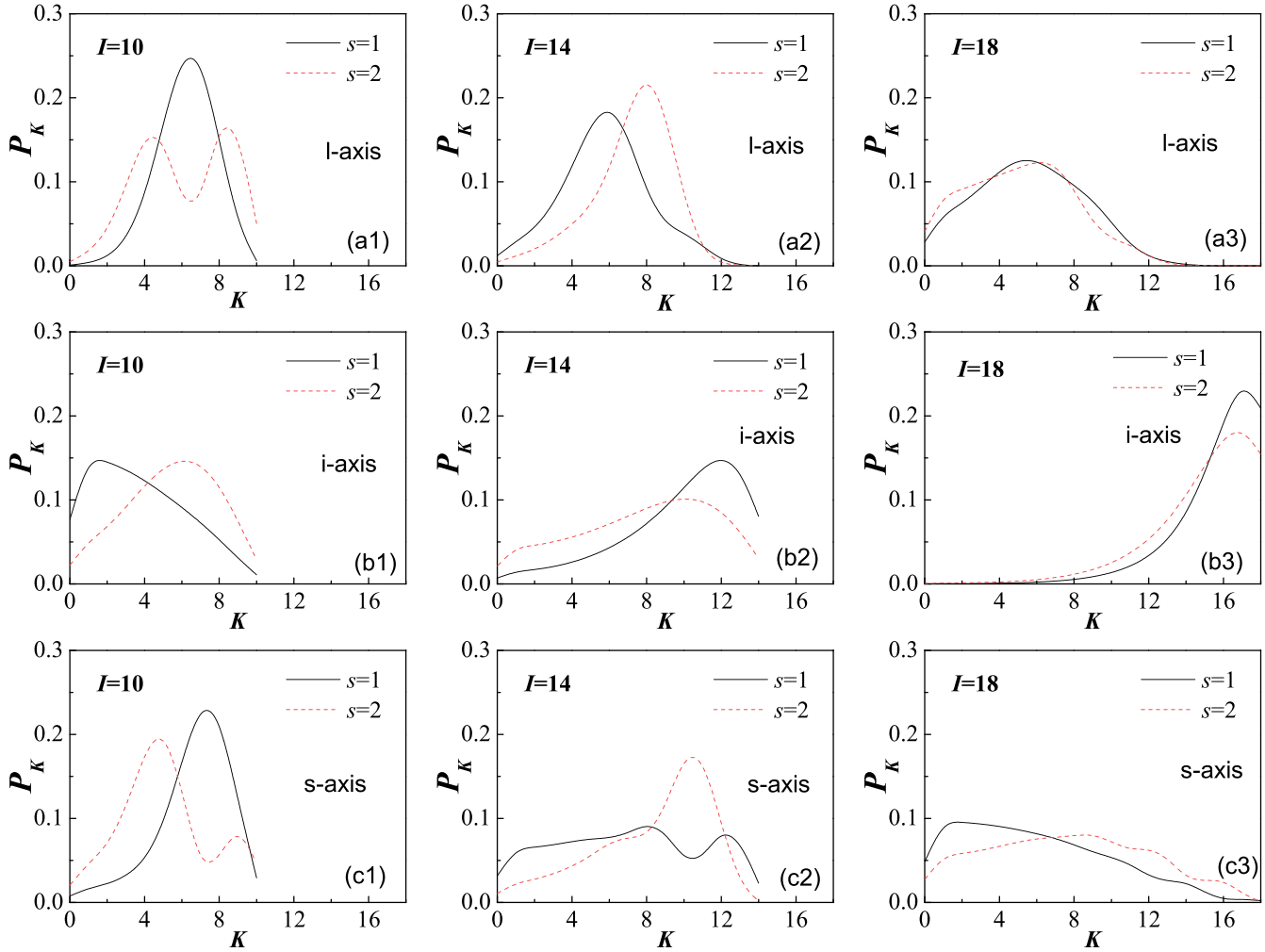

FIG. 8. The probability distributions for the projections K of the total angular momentum along the long (l-), intermediate (i-), and short (s-) axes are presented for $I = 10,\ 14,\ 18$, where $s = 1$ and $s = 2$ denote the results corresponding to the case shown in Fig. 3(a).

Fig. 7(b). This geometric picture of angular momentum coupling is basically consistent with the three-dimensional titled rotation coupling in the doublets bands based on the chiral hypothesis. Apart from that, the calculated results indicate that the core contribution to the total angular momentum could be comparable to the contributions from the valence proton and valence neutron ($h_{11/2}$) [6]. For example, $\overline{L} = \sqrt{\langle |\hat{L}^2| \rangle}$ for two states with $I = 14$ in the doublet bands yield $\overline{L} \approx 6$. This observation also aligns with chiral interpretations [6]. As further seen in Figs. 7(d)–7(f), the evolutional features of the effective angles for $s = 3$ and $s = 4$ are more or less similar to those observed from the $s = 1$ and $s = 2$ doublet bands, suggesting that the two doublets have the similar geometry in angular momentum coupling.

Moreover, the chirality in each doublet bands can be discerned from the probability distribution for the projection of the total angular momentum along the long (l-), intermediate (i-), and short (s-) axes, which coincide with the body-fixed 3, 1, and 2 axes according to the adopted parametrization of γ. Similarly to the effective angles, the probability distribution, referred to as K distribution, is also unaffected by the β part of the wave functions and derived as [93]

$$P_K = \sum_{\Omega_p,\Omega_n} \left| C^{I,K}_{s,\Omega_p,\Omega_n} \right|^2 . \tag{27}$$

To compare the doublet bands denoted by $s = 1,\ 2$ with those denoted by $s = 3,\ 4$, P_K on different axis are calculated for three typical I values ($I = 10,\ 14,\ 18$). The results are presented in Figs. 8 and 9. As seen from Fig. 8, a noticeable difference in the distribution between the $s = 1$ and $s = 2$ bands is observed near the band heads ($I = 10$), consistent with expectations for chiral vibration. Specifically, at low spin ($I = 10$), the maximum distribution on the i-axis appears near $K_{\rm i} = 0$ for $s = 1$, while it occurs at $K_{\rm i} = 6$ for $s = 2$, demonstrating the typical distribution for a chiral vibration between the zero-phonon state ($s = 1$) and one-phonon state ($s = 2$) [57]. With increasing I the distribution of K on the three axes for the two bands are getting closer as indicated by the results for $I = 14$ and $I = 18$, which indicates that the static chirality will develop at higher spins. These features align well with the previous PRM calculations [57], reaffirming the chiral interpretation of the $s = 1$ and $s = 2$ bands. For

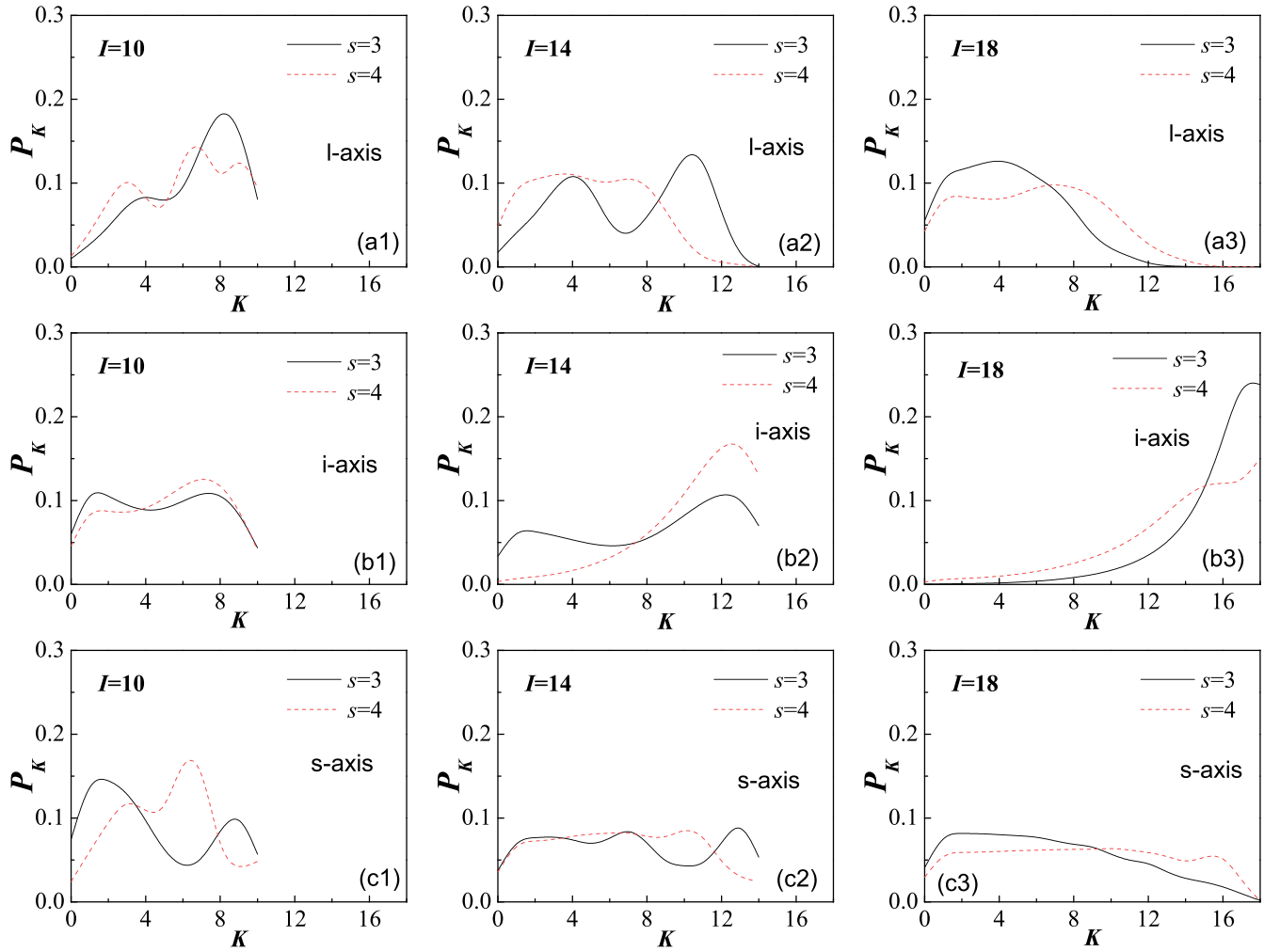

FIG. 9. The same as in Fig. 8 but for $s = 3$ and $s = 4$.

the bands with $s = 3,\ 4$, the evolutions of the distributions of K from low spins to high spins exhibits global similarities to those observed in the bands with $s = 1,\ 2$, particularly along the i-axis. This suggests that the doublet bands $s = 3,\ 4$ can also be attributed to chiral rotation. However, a certain difference between the $s = 3$ and $s = 4$ bands may be sustained even at high spins ($I = 14, 18$) as clearly seen from Fig. 9. This implies that the chiral interpretation of the doublet bands with $s = 3,\ 4$ may not be as robust as that of the bands with $s = 1,\ 2$, despite the more pronounced level degeneracies in the former compared to the latter as seen from Fig. 3(a).

C. Odd-*A* nuclei

As discussed above, the chiral doublet bands in a triaxial odd-odd nucleus with a transitional core can be effectively described within the present model. The phenomenon of wobbling motion provides an alternative perspective for observing triaxiality in nuclei [39]. Specifically, the wobbling mode is characterized by the $\Delta I = 2$ rotational bands connected through $\Delta I = 1, E2$ transitions. Such bands have predominantly been observed in triaxial odd-A nuclei with high-j valence particles. In the following, we select ^{127}Xe and ^{133}La to test the model predictions for the odd-A systems neighboring the even-even core counterparts ^{126}Xe and ^{132}Ba. It is worth noting that the lowest bands built on the single-particle configuration $h_{11/2}$ in the two odd-A nuclei have been proposed as the potential candidates for observing the wobbling mode [50,51]. By fully constraining the parameters based on the core nuclei ^{126}Xe and ^{132}Ba, the level patterns derived from the model are given to compare with those obtained experimentally for ^{127}Xe and ^{133}La as shown in Fig. 10. In the calculations, either $\hat{H}_n$ or $\hat{H}_p$ with the odd particle occupying the $h_{11/2}$ orbit is considered in the model Hamiltonian.

As depicted in Fig. 10(a), the energy levels of the yrast band and side (wobbling) band in ^{127}Xe can be accurately reproduced by the model calculations based on the single-particle configuration $\nu h_{11/2}$. The near degeneracies with $E(I) \approx E(I-1)$ between the two $\Delta I = 2$ bands can be clearly observed from both the experiment data and theoretical predictions, indicating a similar distribution of the moments of inertia for these two rotational bands. Recently, it has been suggested [50] that the side band in this nucleus can be interpreted as a longitudinal wobbling mode of the yrast band. In other words, the two $\Delta I = 2$ bands may group into

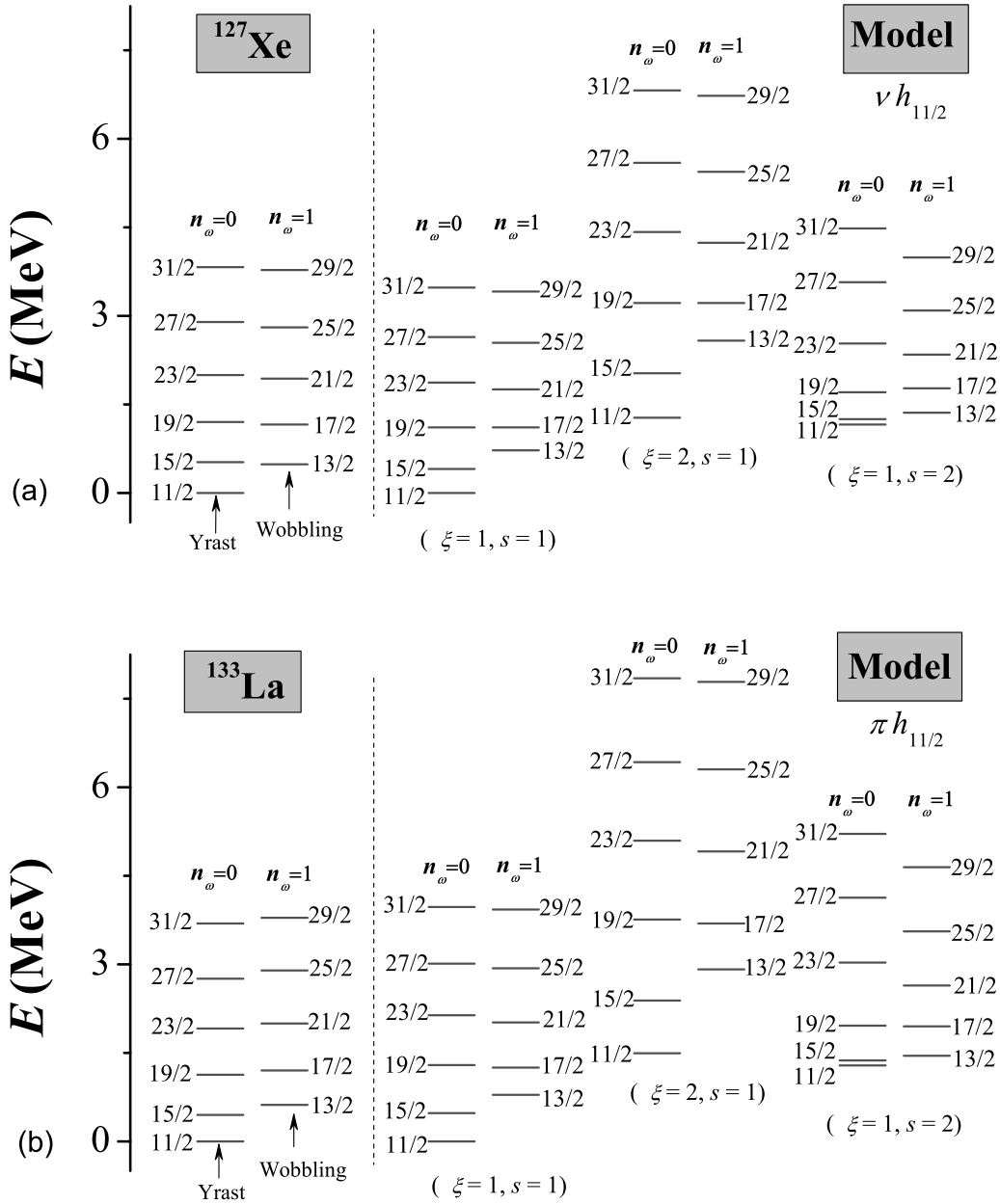

FIG. 10. The patterns of low-lying excitation states for ^{127}Xe [50] and ^{133}La [51] are presented to compare with the results solved from the model Hamiltonian, where $\xi = 1$ and $\xi = 2$ represent the lowest bands and β-vibrational bands, respectively, and $s = 1,\ 2$ is the additional quantum number used to distinguish between states with the same $I,\ M$. In addition, n_ω is introduced to indicate that a $\Delta I = 1$ rotational serial with given $(\xi,\ s)$ may be recognized as two $\Delta I = 2$ bands corresponding to the "ground" band ($n_\omega = 0$) and its wobbling partner ($n_\omega = 1$), respectively (see text).

a rotation-wobbling bands pair corresponding to the wobbling phonon excitations $n_\omega = 0$ and $n_\omega = 1$, respectively. Here, the quantum number n_ω is taken from the harmonic approximation in treating the triaxial rotor model [39] and used to distinguish between two adjacent $\Delta I = 2$ bands for each given (ξ, s) as shown in Fig. 10. A similar picture can also be observed for the odd-proton nucleus, ^{133}La, as seen from Fig. 10(b), where one can observe a good agreement between the experimental data and the theoretical predictions based on the single-particle configuration $\pi h_{11/2}$. Additionally, the results in Fig. 10 indicate that the model can yield a pattern of multiple rotation-wobbling doublets characterized by $n_\omega = 0,\ 1$ with different $(\xi,\ s)$, which bears resemblance to the multiple chiral doublets displayed in Fig. 3. It should be noted that chiral bands have also been observed in odd-A systems [23], but spins in each chiral band change by $\Delta I = 1$ rather than $\Delta I = 2$ as exhibited in a wobbling band.

The wobbling modes can be identified by observing several quantities, including the wobbling energy defined by [42]

$$E_{\rm wob}(I) = E(1, I) - \tfrac{1}{2}[E(0, I-1) + E(0, I+1)] \quad (28)$$

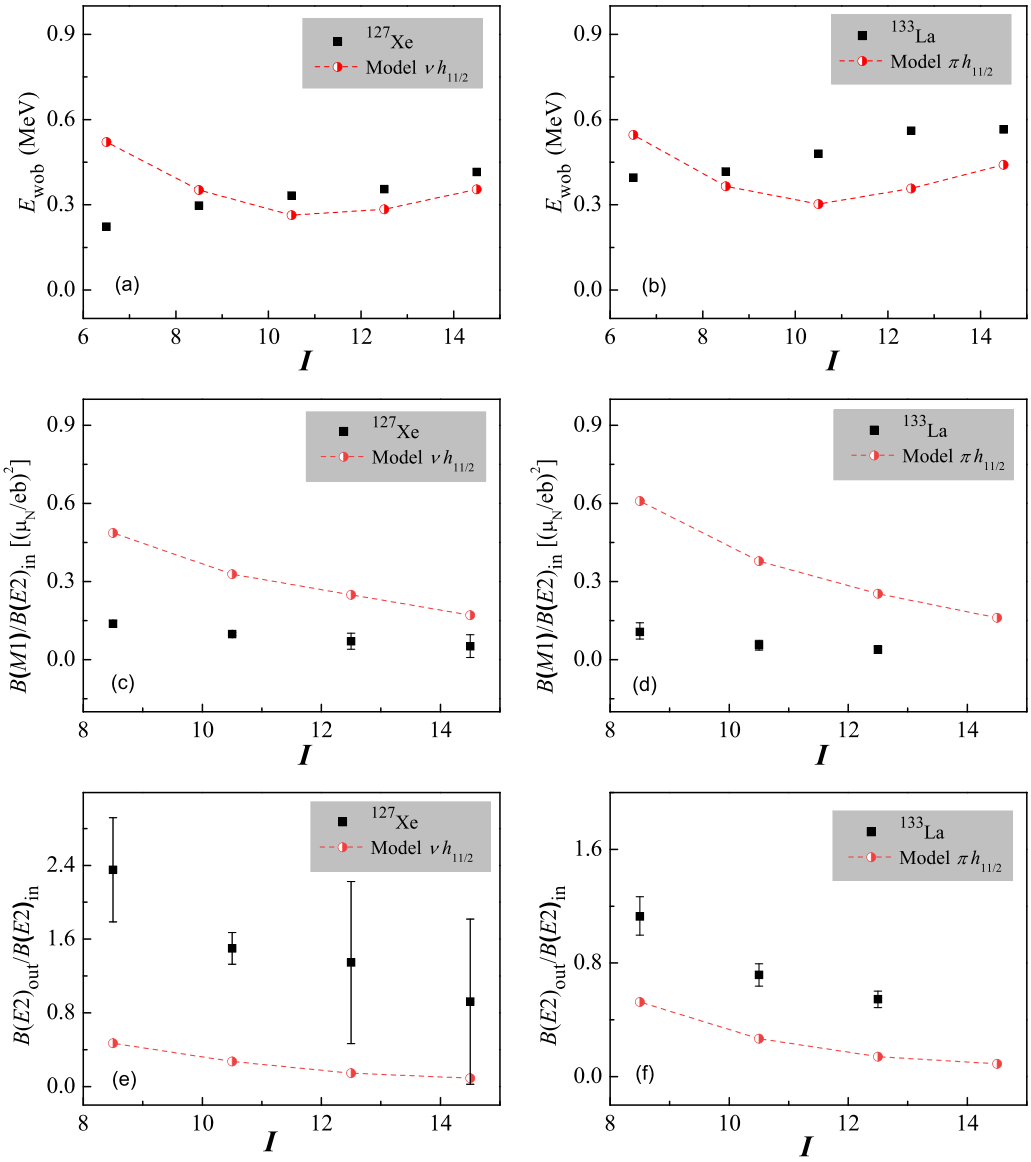

FIG. 11. The available data for E_{wob}, $B(M1)/B(E2)_{in}$ and $B(E2)_{out}/B(E2)_{in}$ in ^{127}Xe [50] and ^{133}La [51] are shown to compare with the results solved from the model Hamiltonian with the assumed single-j configuration.

and the $B(\sigma, \lambda)$ transitional ratios defined by

$$B(M1)/B(E2)_{in} = \frac{B(M1;(1,I)\rightarrow(0,I-1))}{B(E2;(1,I)\rightarrow(1,I-2))}, \quad (29)$$

$$B(E2)_{out}/B(E2)_{in} = \frac{B(E2;(1,I)\rightarrow(0,I-1))}{B(E2;(1,I)\rightarrow(1,I-2))}. \quad (30)$$

In Eqs. (28)–(30), the states are characterized by the quantum numbers (n_ω, I) with $(0, I)$ and $(1, I)$ corresponding to those from the yrast band ($n_\omega = 0$) and its wobbling mode ($n_\omega = 1$), respectively. As shown in the Fig. 11(a), the E_{wob} values extracted from ^{127}Xe may increase with spins, suggesting a longitudinal wobbling mode in this nucleus [50]. This trend is qualitatively captured by the model calculations, particularly for high-spin states. The similar situation can also be observed for ^{133}La as seen in Fig. 11(b). For $B(M1)/B(E2)_{in}$ and $B(E2)_{out}/B(E2)_{in}$, the results presented in Figs. 11(c)–11(f) indicate that the available data can also be qualitatively explained from the model calculations for both nuclei, but some quantitative deviations are evident. For instance, the model predictions heavily underestimate the $B(E2)_{out}/B(E2)_{in}$ in ^{127}Xe especially at low spins. Adopting a larger γ value may improve this $B(E2)$ ratio at specific spins; for example, setting $\gamma = 30^\circ$ would elevate $B(E2)_{out}/B(E2)_{in}$ at $I = 17/2$ from the current value of 0.47 to 0.88. Nonetheless, a quantitative description of the large ratio values in ^{127}Xe, which are also much larger than those observed in ^{133}La as depicted in Fig. 11(f), may go beyond the simple model calculations with the parameters fully determined from fitting the core nucleus. A better descriptions of $B(E2)_{out}/B(E2)_{in}$ in experiments can be achieved from the PRM calculations with the assumed spin-dependent moments of inertia [51]. But, the resulting $B(M1)/B(E2)_{in}$ ratio will be significantly larger than the relevant data [42,49,53] as well as the results derived from the

present model. For example, $B(M1)/B(E2)_{\rm in}$ at $I = 17/2$ in the present model calculation for ^{133}La is given by 0.61 (in μ_N^2/e^2b^2) as shown in Fig. 11(d), while the PRM calculations with the spin-dependent moments of inertia [51] will yield the ratio value larger than 1.4. While a quenching factor was often introduced in the PRM calculations [49] to improve agreement with small experimental $B(M1)/B(E2)_{\rm in}$ ratio, the present model provides a relatively reasonable theoretical description without requiring such adjustments, despite the fact that the data are still overestimated by the calculated results, as illustrated in Fig. 11.

Based on the aforementioned discussions, the two bands characterized by ($\xi = 1$, $s = 1$) as depicted in Fig. 10 can be elucidated as a pair of rotation-wobbling doublet consisting of a $\Delta I = 2$ rotational band identify by $n_\omega = 0$ and its wobbling partner designated by $n_\omega = 1$. To further discern the wobbling nature of other bands in the model, we employ the case presented in Fig. 10(a) as an example to compare the doublet denoted by ($\xi = 1$, $s = 1$) with those denoted by ($\xi = 2$, $s = 1$) and ($\xi = 1$, $s = 2$). Specifically, the quantities defined in Eqs. (28)–(30) have been calculated for each doublet and the results as a function of spin are presented in Fig. 12. In the calculations, the band built on $I = 13/2$ has been assigned as the $n_\omega = 1$ mode of that built on $I = 11/2$ in each doublet. As observed from Fig. 12(a), the evolutional behavior of $E_{\rm wob}$ for ($\xi = 2$, $s = 1$) closely resembles that for ($\xi = 1$, $s = 1$) but differs from the one for ($\xi = 1$, $s = 2$). The similarity between the two pairs of bands with $s = 1$ are even highlighted by the results for $B(M1)/B(E2)_{\rm in}$ and $B(E2)_{\rm out}/B(E2)_{\rm in}$ as seen in Fig. 12. It is thus inferred that the wobbling motion can not only be effectively preserved in a transitional system but also robust against β vibrations. This observation is similar to the above discussed chiral rotation. It should be mentioned that the band built on $I = 13/2$ with ($\xi = 1\, s = 2$,) cannot be considered as the $n_\omega = 2$ wobbling mode of the yrast band due to almost zero interband $E2$ transitions, which means that the two $\Delta I = 2$ bands are not $E2$ connected.

To further identify the geometry of angular momentum in the wobbling modes, we calculate the root-mean-square values of the angular momentum components, $\langle I_k^2\rangle^{1/2}$, where I_k with $k = 1, 2, 3$ represents the projection of the total angular momentum I on the body-fixed k axis with $\langle I_1^2\rangle + \langle I_2^2\rangle + \langle I_3^2\rangle = I(I+1)$. Given that the β part of the wave functions only contributes an orthonormality factor, the calculated results would be identical for the states with the same values of s and I. This suggests that the angular momentum geometry in the present model is solely determined by the quantum numbers s and n_ω, rather than by ξ. Hence, a meaningful comparison should be conducted between two bands with identical s but different n_ω. As seen in Fig. 13(a), the results indicate that at high spins such as $I > 23/2$, the angular momenta in the two bands with $s = 1$ will be predominantly influenced by their $k = 1$ components. Notably, it is observed that the $k = 1$ components in the $n_\omega = 0$ band exceed those in the $n_\omega = 1$ band (wobbling mode) by nearly an average of $1\hbar$. For instance, if one defines the spin difference by

$$\overline{\Delta I_k} = \langle I_k^2\rangle_{n_\omega=0}^{1/2} - \frac{\langle (I+1)_k^2\rangle_{n_\omega=1}^{1/2} + \langle (I-1)_k^2\rangle_{n_\omega=1}^{1/2}}{2}, \quad (31)$$

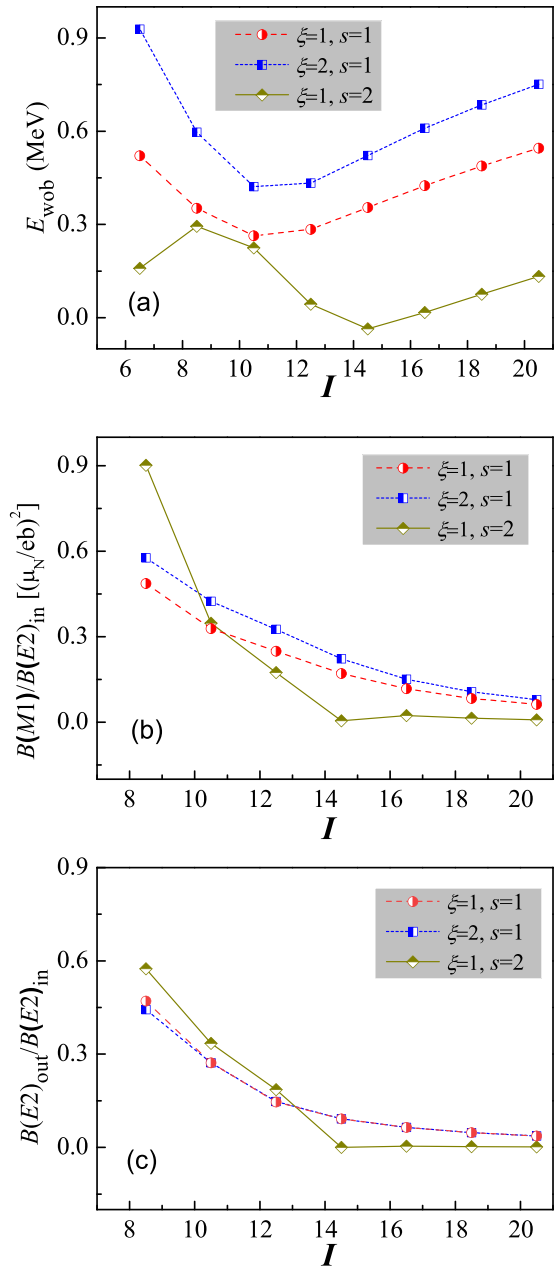

FIG. 12. The theoretical values of $E_{\rm wob}$, $B(M1)/B(E2)_{\rm in}$ and $B(E2)_{\rm out}/B(E2)_{\rm in}$ are presented as a function of I for the bands depicted in Fig. 10(a).

then one may get $\overline{\Delta I_1} \approx 0.8\hbar$ for $I = 27/2$ and $\overline{\Delta I_1} \approx 0.7\hbar$ for $I = 35/2$, respectively. This is consistent with the description [39] that the wobbling motion describes small amplitude oscillation of the total angular momentum vector with respect to the principal axis with the largest moment of inertia, which coincides with the $k = 1$ axis in the present model. As further demonstrated in Fig. 13(b), the similar angular momentum geometry can also be identified for the two bands with $s = 2$, particularly for high-spin states such as those with $I > 27/2$. Therefore, it is reasonable to distribute the band built on $I = 13/2$ as the $n_\omega = 1$ mode of that built on $I = 11/2$, as indicated in Fig. 10.

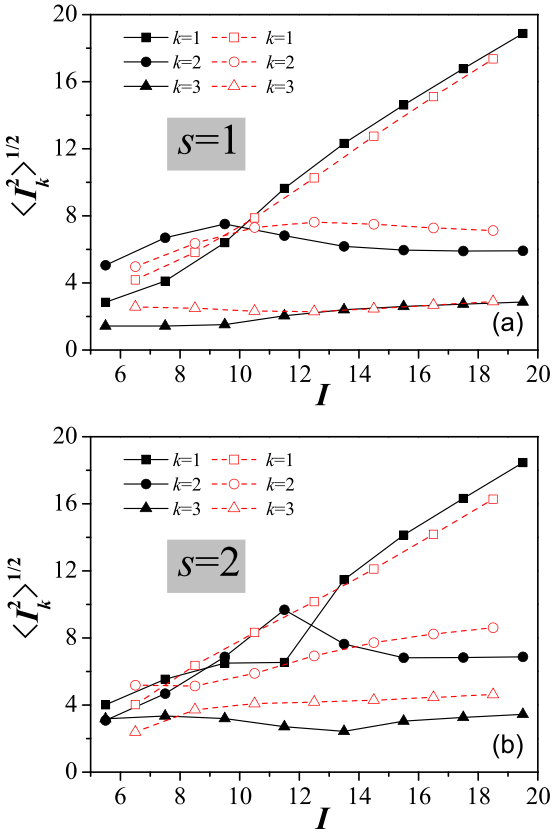

FIG. 13. The root-mean-square values (in $\hbar$) of the angular momentum components, $\langle I_k^2 \rangle^{1/2}$ with $k = 1, 2, 3$, are presented as a function of I for the $n_\omega = 0$ (full and black symbols) and $n_\omega = 1$ (empty and red symbols) bands depicted in Fig. 10(a). Since the calculated values are independent of the ξ number (as discussed in the text), only $s = 1$ and $s = 2$ are used to denote the results for each rotation-wobbling pair.

IV. SUMMARY

In summary, a collective model incorporating the β-soft potential has been developed within the core-particle coupling scheme. This extends the original PRM description of triaxial dynamics to the β-soft case. It is demonstrated that the model can be solved through approximately separating the β variable describing collective vibration from the Euler angles describing collective rotation. The obtained solutions are expressed in terms of the Bessel functions of irrational orders and subsequently applied to analyze the relevant nuclei in $A \approx 130$ mass region. The results indicate that chiral doublet bands and wobbling bands in the odd nuclei can be reasonably explained by the model calculations with the parameters completely determined from fitting the neighboring even-even nuclei. This suggests that triaxial dynamics in an transitional even-even system can be well preserved in its adjacent odd partners, although the manifestation of triaxiality differ significantly between odd and even species. Additionally, the model presents a picture of multiple chiral doublets or multiple rotation-wobbling doublets caused by collective excitations, demonstrating a new possibility of producing multiple-bands pattern in odd systems. Since the early prediction of the multiple chiral doublets based on multiple single-particle configurations [24], searching for the possible candidates has become an active issue in experiments [28–38]. Most recently, it was found [54] that the chiralilty and wobbling modes can even coexist in a single nucleus, which provides new insights into observing multiple chiral doublets in triaxial systems. The proposed multiple doublets caused by collective excitations are different from those previously predicted based on several single-particle configurations [24] or an identical configuration [29]. However, whether the present predictions can be confirmed experimentally needs more careful and systematic analysis of the relevant data. In particular, it would be beneficial to find a way to treat the parameter γ as a degree of freedom [94–96] rather than to keep it frozen as in the analysis presented in the current paper. The related work is in progress.

ACKNOWLEDGMENTS

Fruitful discussions with Q. B. Chen, Z. P. Li, J. Meng, Y. Y. Wang, S. Q. Zhang, and P. W. Zhao are acknowledged. Support from the National Natural Science Foundation of China (Grant No. 12375113) is acknowledged.

[1] S. Frauendorf, Rev. Mod. Phys. **73**, 463 (2001).
[2] S. Frauendorf and J. Meng, Nucl. Phys. A **617**, 131 (1997).
[3] K. Starosta, T. Koike, C. J. Chiara, D. B. Fossan, D. R. LaFosse, A. A. Hecht *et al.*, Phys. Rev. Lett. **86**, 971 (2001).
[4] T. Koike, K. Starosta, C. J. Chiara, D. B. Fossan, and D. R. LaFosse, Phys. Rev. C **63**, 061304(R) (2001).
[5] R. A. Bark *et al.*, Nucl. Phys. A **691**, 577 (2001).
[6] K. Starosta, C. J. Chiara, D. B. Fossan, T. Koike, T. T. S. Kuo, D. R. LaFosse *et al.*, Phys. Rev. C **65**, 044328 (2002).
[7] E. Mergel *et al.*, Eur. Phys. J. A **15**, 417 (2002).
[8] T. Koike, K. Starosta, C. J. Chiara, D. B. Fossan, and D. R. LaFosse, Phys. Rev. C **67**, 044319 (2003).
[9] S. Zhu *et al.*, Phys. Rev. Lett. **91**, 132501 (2003).
[10] S. Y. Wang, Y. Z. Liu, T. Komatsubara, Y. J. Ma, and Y. H. Zhang, Phys. Rev. C **74**, 017302 (2006).
[11] E. Grodner, J. Srebrny, A. A. Pasternak, I. Zalewska, T. Morek, Ch. Droste *et al.*, Phys. Rev. Lett. **97**, 172501 (2006).
[12] D. Tonev, G. de Angelis, P. Petkov, A. Dewald, S. Brant, S. Frauendorf *et al.*, Phys. Rev. Lett. **96**, 052501 (2006).
[13] P. Joshi, M. P. Carpenter, D. B. Fossan, T. Koike, E. S. Paul, G. Rainovski, K. Starosta, C. Vaman, and R. Wadsworth, Phys. Rev. Lett. **98**, 102501 (2007).
[14] E. A. Lawrie, P. A. Vymers, J. J. Lawrie, Ch. Vieu, R. A. Bark, R. Lindsay *et al.*, Phys. Rev. C **78**, 021305(R) (2008).
[15] J. Timár, C. Vaman, K. Starosta, D. B. Fossan, T. Koike, D. Sohler, I. Y. Lee, and A. O. Macchiavelli, Phys. Rev. C **73**, 011301(R) (2006).

[16] C. Vaman, D. B. Fossan, T. Koike, K. Starosta, I. Y. Lee, and A. O. Macchiavelli, Phys. Rev. Lett. **92**, 032501 (2004).
[17] P. Joshi *et al.*, Phys. Lett. B **595**, 135 (2004).
[18] J. Timár *et al.*, Phys. Lett. B **598**, 178 (2004).
[19] J. A. Alcántara-Núñez *et al.*, Phys. Rev. C **69**, 024317 (2004).
[20] D. L. Balabanski, M. Danchev, D. J. Hartley, L. L. Riedinger, O. Zeidan, J. Y. Zhang *et al.*, Phys. Rev. C **70**, 044305 (2004).
[21] S. Y. Wang *et al.*, Phys. Lett. B **703**, 40 (2011).
[22] E. Grodner *et al.*, Phys. Lett. B **703**, 46 (2011).
[23] B. W. Xiong and Y. Y. Wang, At. Data Nucl. Data Tables **125**, 193 (2019).
[24] J. Meng, J. Peng, S. Q. Zhang, and S. G. Zhou, Phys. Rev. C **73**, 037303 (2006).
[25] J. Peng, H. Sagawa, S. Q. Zhang, J. M. Yao, Y. Zhang, and J. Meng, Phys. Rev. C **77**, 024309 (2008).
[26] J. M. Yao, B. Qi, S. Q. Zhang, J. Peng, S. Y. Wang, and J. Meng, Phys. Rev. C **79**, 067302 (2009).
[27] J. Li, S. Q. Zhang, and J. Meng, Phys. Rev. C **83**, 037301 (2011).
[28] A. D. Ayangeakaa, U. Garg, M. D. Anthony, S. Frauendorf, J. T. Matta, B. K. Nayak *et al.*, Phys. Rev. Lett. **110**, 172504 (2013).
[29] I. Kuti *et al.*, Phys. Rev. Lett. **113**, 032501 (2014).
[30] C. Liu, S. Y. Wang, R. A. Bark, S. Q. Zhang, J. Meng, B. Qi *et al.*, Phys. Rev. Lett. **116**, 112501 (2016).
[31] D. Tonev, M. S. Yavahchova, N. Goutev, G. de Angelis, P. Petkov, R. K. Bhowmik *et al.*, Phys. Rev. Lett. **112**, 052501 (2014).
[32] E. O. Lieder, R. M. Lieder, R. A. Bark, Q. B. Chen, S. Q. Zhang, J. Meng *et al.*, Phys. Rev. Lett. **112**, 202502 (2014).
[33] N. Rather *et al.*, Phys. Rev. Lett. **112**, 202503 (2014).
[34] C. M. Petrache, B. F. Lv, A. Astier, E. Dupont, Y. K. Wang, S. Q. Zhang *et al.*, Phys. Rev. C **97**, 041304(R) (2018).
[35] T. Roy *et al.*, Phys. Lett. B **782**, 768 (2018).
[36] B. Qi, H. Jia, C. Liu, and S. Y. Wang, Sci. China Phys. Mech. Astron. **62**, 12012 (2019).
[37] S. Guo *et al.*, Phys. Lett. B **807**, 135572 (2020).
[38] B. F. Lv, C. M. Petrache, Q. B. Chen, J. Meng, A. Astier, E. Dupont *et al.*, Phys. Rev. C **100**, 024314 (2019).
[39] A. Bohr and B. R. Mottelson, *Nucear Structure* (Benjamin, New York, 1975), Vol. II.
[40] I. Hamamoto, Phys. Rev. C **65**, 044305 (2002).
[41] I. Hamamoto and G. B. Hagemann, Phys. Rev. C **67**, 014319 (2003).
[42] S. Frauendorf and F. Dönau, Phys. Rev. C **89**, 014322 (2014).
[43] S. W. Ødegård, G. B. Hagemann, D. R. Jensen, M. Bergström, B. Herskind, G. Sletten *et al.*, Phys. Rev. Lett. **86**, 894 (2001).
[44] G. Schönwaßer *et al.*, Phys. Lett. B **552**, 9 (2003).
[45] H. Amro *et al.*, Phys. Lett. B **553**, 197 (2003).
[46] P. Bringel *et al.*, Eur. Phys. J. A **24**, 167 (2005).
[47] D. J. Hartley, R. V. F. Janssens, L. L. Riedinger, M. A. Riley, A. Aguilar, M. P. Carpenter *et al.*, Phys. Rev. C **80**, 041304(R) (2009).
[48] J. T. Matta, U. Garg, W. Li, S. Frauendorf, A. D. Ayangeakaa, D. Patel *et al.*, Phys. Rev. Lett. **114**, 082501 (2015).
[49] J. Timár, Q. B. Chen, B. Kruzsicz, D. Sohler, I. Kuti, S. Q. Zhang *et al.*, Phys. Rev. Lett. **122**, 062501 (2019).
[50] S. Chakraborty *et al.*, Phys. Lett. B **811**, 135854 (2020).
[51] S. Biswas *et al.*, Eur. Phys. J. A **55**, 159 (2019).
[52] N. Sensharma, U. Garg, Q. B. Chen, S. Frauendorf, D. P. Burdette, J. L. Cozzi *et al.*, Phys. Rev. Lett. **124**, 052501 (2020).
[53] S. Nandi, G. Mukherjee, Q. B. Chen, S. Frauendorf, R. Banik, S. Bhattacharya *et al.*, Phys. Rev. Lett. **125**, 132501 (2020).
[54] R. J. Guo, S. Y. Wang, C. Liu, R. A. Bark, J. Meng, S. Q. Zhang *et al.*, Phys. Rev. Lett. **132**, 092501 (2024).
[55] J. Peng, J. Meng, and S. Q. Zhang, Phys. Rev. C **68**, 044324 (2003).
[56] S. Q. Zhang, B. Qi, S. Y. Wang, and J. Meng, Phys. Rev. C **75**, 044307 (2007).
[57] B. Qi, S. Q. Zhang, S. Y. Wang, J. M. Yao, and J. Meng, Phys. Rev. C **79**, 041302(R) (2009).
[58] V. I. Dimitrov, S. Frauendorf, and F. Dönau, Phys. Rev. Lett. **84**, 5732 (2000).
[59] P. Olbratowski, J. Dobaczewski, J. Dudek, and W. Plóciennik, Phys. Rev. Lett. **93**, 052501 (2004).
[60] S. Mukhopadhyay, D. Almehed, U. Garg, S. Frauendorf, T. Li, P. V. Madhusudhana Rao *et al.*, Phys. Rev. Lett. **99**, 172501 (2007).
[61] S. Brant, D. Tonev, G. de Angelis, and A. Ventura, Phys. Rev. C **78**, 034301 (2008).
[62] K. Nomura, R. Rodríguez-Guzmán, and L. M. Robledo, Phys. Rev. C **101**, 014306 (2020).
[63] F. Q. Chen, Q. B. Chen, Y. A. Luo, J. Meng, and S. Q. Zhang, Phys. Rev. C **96**, 051303(R) (2017).
[64] F. Q. Chen, J. Meng, and S. Q. Zhang, Phys. Lett. B **785**, 211 (2018).
[65] E. Streck, Q. B. Chen, N. Kaiser, and UIf-G. Meißner, Phys. Rev. C **98**, 044314 (2018).
[66] K. Tanabe and K. Sugawara-Tanabe, Phys. Rev. C **95**, 064315 (2017).
[67] R. Budaca, Phys. Rev. C **97**, 024302 (2018).
[68] A. A. Raduta, R. Poenaru, and C. M. Raduta, Phys. Rev. C **101**, 014302 (2020).
[69] Q. B. Chen, S. Q. Zhang, and J. Meng, Phys. Rev. C **94**, 054308 (2016).
[70] M. Matsuzaki and S. I. Ohtsubo, Phys. Rev. C **69**, 064317 (2004).
[71] Y. R. Shimizu, T. Shoji, and M. Matsuzaki, Phys. Rev. C **77**, 024319 (2008).
[72] L. Fortunato, Eur. Phys. J. A **26**, 1 (2005).
[73] F. Iachello, Phys. Rev. Lett. **85**, 3580 (2000).
[74] F. Iachello, Phys. Rev. Lett. **87**, 052502 (2001).
[75] D. Bonatsos, D. Lenis, D. Petrellis, and P. A. Terziev, Phys. Lett. B **588**, 172 (2004).
[76] D. Bonatsos, D. Lenis, D. Petrellis, P. A. Terziev, and I. Yigitoglu, Phys. Lett. B **621**, 102 (2005).
[77] Y. Zhang, F. Pan, Y. A. Luo, and J. P. Draayer, Phys. Lett. B **751**, 423 (2015).
[78] R. Budaca and A. I. Budaca, Phys. Lett. B **759**, 349 (2016).
[79] P. Ring and P. Schuck, *The Nuclear Many-Body Problem* (Springer-Verlag, Berlin 1980).
[80] Y. Zhang, F. Pan, Y. X. Liu, Y. A. Luo, and J. P. Draayer, Phys. Rev. C **96**, 034323 (2017).
[81] A. S. Davydov and A. A. Chaban, Nucl. Phys. **20**, 499 (1960).
[82] H. Zhang, B. Qi, X. D. Wang, H. Jia, and S. Y. Wang, Phys. Rev. C **105**, 034339 (2022).
[83] J. Hu, S. Y. An, and Y. Zhang, J. Phys. G **46**, 045101 (2019).
[84] A. A. Sonzogni, Nucl. Data Sheets **95**, 837 (2002); **103**, 1 (2004).
[85] Y. Khazov, A. A. Rodionov, S. Sakharov, and B. Singh, Nucl. Data Sheets **104**, 497 (2005).
[86] B. Singh, Nucl. Data Sheets **93**, 33 (2001).

[87] M. Kanbe and K. Kitao, Nucl. Data Sheets **94**, 227 (2001).
[88] J. Katakura and K. Kitao, Nucl. Data Sheets **97**, 765 (2002).
[89] H. Iimura, J. Katakura, K. Kitao, and T. Tamura, Nucl. Data Sheets **80**, 895 (1997).
[90] A. Gade, I. Wiedenhöver, H. Meise, A. Gelberg, and P. von Brentano, Nucl. Phys. A **697**, 75 (2002).
[91] E. Grodner, J. Phys.: Conf. Ser. **366**, 012022 (2012).
[92] S. Y. Wang, S. Q. Zhang, B. Qi, and J. Meng, Phys. Rev. C **75**, 024309 (2007).
[93] B. Qi, S. Q. Zhang, J. Meng, S. Y. Wang, and S. Frauendorf, Phys. Lett. B **675**, 175 (2009).
[94] K. Higashiyama and N. Yoshinaga, Eur. Phys. J. A **33**, 355 (2007).
[95] Ch. Droste, S. G. Rohoziński, K. Starosta, L. Próchniak, and E. Grodner, Eur. Phys. J. A **42**, 79 (2009).
[96] Y. Zhang, B. Qi, and S. Q. Zhang, Sci. China Phys. Mech. Astron. **64**, 122011 (2021).